Paleoclimatic reconstruction in the Tatra Mountains of the western Carpathians during MIS 9–7 inferred from a multiproxy speleothem record

Marcin Błaszczyk[a]* , Helena Hercman[a], Jacek Pawlak[a], Jacek Szczygieł[b]

[a]Institute of Geological Sciences, Polish Academy of Sciences, Twarda 51/55, 00-818 Warszawa, Poland
[b]Institute of Earth Sciences, University of Silesia, Będzińska 60, 41-200 Sosnowiec, Poland
*Corresponding author at: Institute of Geological Sciences, Polish Academy of Sciences, Twarda 51/55, 00-818 Warszawa, Poland.
E-mail address: marcin.blaszczyk@twarda.pan.pl (M. Błaszczyk).

Abstract

The SC-3 speleothem from Szczelina Chochołowska Cave, located in the Tatra Mountains, was studied in detail. U-series dating and age–depth modeling allowed us to constrain the period of speleothem growth to between approximately 330 and 200 ka, that is, during Marine Isotope Stages (MIS) 9–7. The complementary use of stable isotope analyses, petrographic studies, and trace element analyses allowed the identification of warm and wet climatic conditions that were favorable for speleothem growth during MIS 9e and MIS 9c. Unfavorable climatic periods included the cold glacial conditions of MIS 8 and the MIS 9/MIS 8 transition. The breaks in the growth of the SC-3 stalagmite were most likely connected with a reduction in precipitation in MIS 9a and extreme hydrologic events during MIS 8. Comparisons with other European records suggest that the climatic variability recorded in the speleothem from the Tatra Mountains is not only a record of local environmental conditions but can also be linked to European climatic patterns during both interglacial and glacial intervals. This makes our study the northernmost paleoclimatic record for the whole Carpathian range and one of the very few records from those periods worldwide.

Keywords: Speleothem; Paleoclimate; MIS 9–7; Stable isotopes; Speleothem fabrics; Trace elements; Tatra Mountains; Western Carpathians

INTRODUCTION

The middle Pleistocene climate was characterized by very intense glaciations alternating with long, warm interglaciations. Tracking glacial–interglacial cycles and their impacts on terrestrial environments is a challenging task for Quaternary science, largely due to a lack of precisely dated sediment records of the advance and retreat of middle Pleistocene ice sheets. During the middle Pleistocene, Poland was occupied by ice sheets from five Scandinavian glaciations, and the most extensive glaciations passed over the South Poland Uplands and entered the Czech Republic. Apart from the Scandinavian ice sheet, mountain glaciers also developed in the Carpathian and Sudetes Mountains (Marks, 2011).

Biological remains of this period in northern continental Europe are scarce, and climatic reconstructions mostly rely on lithological and morphological evidence. Some of the best available sources of paleoclimatic information are speleothems, but until now there have been only a few high-resolution European and Near Eastern speleothem records older than the last interglaciation (Ayalon et al., 2002; Bard et al., 2002; Bar-Matthews et al., 2003; Drysdale et al., 2004; Spötl and Mangini, 2007; Spötl et al., 2008; Columbu et al., 2018; Regattieri et al., 2018).

Previous studies have identified speleothems older than the last interglaciation from the Tatra Mountains, Poland, which formed between MIS 9 and MIS 6, but no detailed paleoclimatic reconstruction was performed (Hercman et al., 1998, 2008; Kicińska et al., 2017). Recently in that area, a stable isotope analysis of speleothem calcite was used to study the age and activity of slope failures (Szczygieł et al., 2019). Phreatic speleothems, including massive rafts, that began to grow during MIS 7 were also found in the Klęczany Quarry (Polish western Carpathians; Gradziński et al., 2012).

Analyses of their structures, ages, and stable isotope compositions were conducted to explain their formation (Gradziński et al., 2012), but these analyses were not used for paleoclimatic reconstruction.

In this study, we present a new paleoclimatic record based on the stable isotope composition, petrography, and trace element content of a stalagmite collected from the Tatra Mountains, southern Poland. The new record spans MIS 9 to 7 (ca. 330–200 ka) and is one the few paleoenvironmental records of the MIS 9 interglaciation from central Europe. MIS 9 was a warm period with some similarities to the Holocene (Ruddiman, 2007) and has been considered a possible analog to the future human-induced warm climate (Yin and Berger, 2015). Such study of past climates is important for improving our understanding of natural climatic fluctuations. This study, as the first comprehensive paleoclimatic study based on Tatra speleothems, has regional importance, because glaciations before the last glacial period are poorly recognized (Kłapyta and Zasadni, 2018). Furthermore, we provide a multiproxy paleoclimatic study on the northern slopes of the Carpathians during the middle Pleistocene, a region and period that are still poorly represented, especially in European continental archives (Kern et al., 2019).

CAVE SETTINGS

Study area

The Tatra Mountains are the highest range of the Carpathians, reaching 2655 m above sea level (asl; Fig. 1). Elevated 1600 m above their surroundings and shaped by glaciers, the Tatra Mountains have alpine characteristics in terms of both geomorphology and ecology. Outcropping to the south, the crystalline basement is covered by Mesozoic sediments and thrust nappes, which are exposed in the northern and westernmost parts of the massif (Jurewicz, 2005). The sedimentary succession is composed mostly of carbonates affected by karstic erosion, which has resulted in karst drainage developments, including numerous caves (Gradziński et al., 2009). We studied a speleothem from Szczelina Chochołowska Cave (49° 14′45.40″N, 19°48′43.14″E) located in the Chochołowska Valley.

The Chochołowska Valley is located in the northwestern portion of the Tatra Mountains (Fig. 1). On the border between crystalline and carbonate rocks, part of the water was captured by karst, and underground drainage dissolved the conduits of Szczelina Chochołowska Cave, the longest cave in the valley (2320 m long; Luty, 2013; Fig. 2A). A more detailed study of the Szczelina Chocholowska Cave geologic setting and its development was presented by Nowicki (1996). The hydrological connections of the cave and the results of dye-tracer experiments in that area were described by Barczyk (2004). The cave is horizontal, with three entrances at 1051, 1072, and 1083 m asl (i.e., 26, 50, and 51 m above the valley bottom), and is developed mainly in Upper Jurassic–Lower Cretaceous limestone and partly in crinoid Middle Jurassic limestone (Borówka et al., 1985;

Nowicki, 1996). Hitherto, the oldest speleothem dated from Szczelina Chochołowska Cave was approximately 350 ka (Hercman et al., 1998). The stalagmite (SC-3) was collected in the New Corridor (Hercman et al., 1998; Fig. 2A).

Local climate and isotopic studies in the Tatra Mountains

Poland lies in the center of Europe, and it has been shown that the Polish climate roughly represents the average climate of Europe (e.g., Luterbacher et al. 2010). A very good agreement between European land (excluding Poland) and Polish winter temperatures (at interannual and interdecadal time scales) was reported; the correlation coefficient of Polish and European mean temperatures over the last full 500 year period was 0.96. Precipitation was more variable than temperature during that time period; however, the results also indicated that the reconstructed winter precipitation over Poland agrees well with those for the rest of Europe (Luterbacher et al. 2010). The North Atlantic Oscillation in Poland, as in western Europe, is the most important large-scale source of climatic variability. The confirmed stability of the large- to regional-scale links is very important for all paleoclimatic reconstruction works, because the robustness of the link between a local proxy and the large-scale climate is a necessary condition for the correct interpretation of different climatic proxies. However, the research area is located in the mountains, so local conditions strongly influence the extraregional climatic pattern observed in the Polish lowlands. In particular, it is related to the temperature gradient, which is approximately 0.6°C per 100 m in the Tatra Mountains, and to the increased total annual sum of precipitation. The Tatra Mountains are located in a transitional climatic zone under the influence of polar–oceanic humid air masses. The distribution of the mean annual temperature is nearly uniform on the northern and southern slopes of the massif, with only slightly higher values, approximately 0.5°C, on the southern slope (Makos et al., 2014).

For the last 50 years in Chochołowska Valley, the maximum and minimum absolute temperatures recorded are 30.0°C and −32.1°C, respectively. Based on data collected from 1951, in that region, the coldest temperatures are usually in January, and the warmest month is July. The mean temperatures are −5.7°C for winter and 12.3°C for summer, and the mean annual temperature is 3.6°C (Niedźwiedź, 1992).

The annual precipitation at the same elevation of the Tatra Mountains massif is approximately 40% higher on the northern slopes than on the southern slopes. This is due to the prevailing northwestern atmospheric circulation and moisture transport in central Europe (Niedźwiedź, 1992). The annual precipitation on the northern slope of the Tatra Mountains is 1100 mm in Zakopane (850 m asl), 1788 mm in Hala Gąsienicowa (1520 m asl), and 1800 mm in Kasprowy Wierch (1991 m asl; Makos et al., 2014). The annual total precipitation amount at the Chochołowska Valley meteorological station is approximately 1300 mm, with much higher
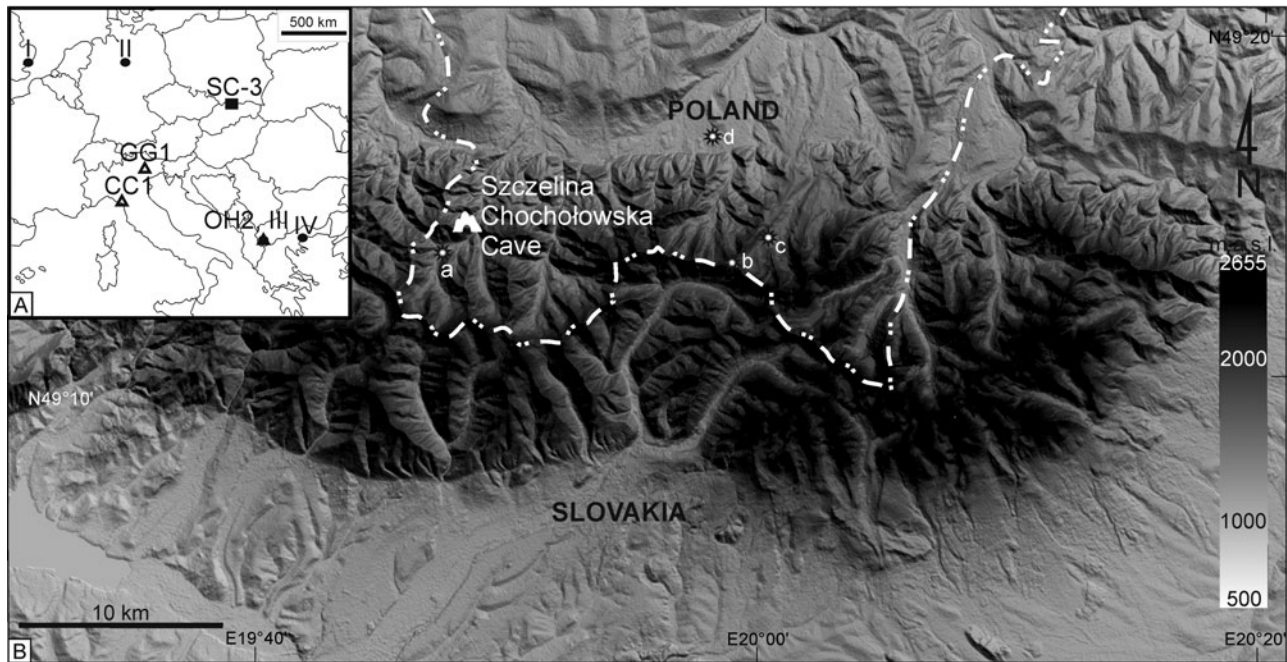
Figure 1. Location of the study site. (A) Location of selected speleothems from Europe: OH2 (Regattieri et al., 2018); GG1 (Columbu et al., 2018); and CC1 (Drysdale et al., 2004) marked as black triangles; location of other records: I, the southeastern Essex channel deposits (Roe et al., 2009); II, pollen records from northern Germany (Urban, 2007); III, pollen records from Lake Ohrid (Sadori et al., 2016); IV, pollen records from northeastern Greece (Fletcher et al., 2013); location of SC-3 in the Tatra Mountains (black rectangle); (B) location of Szczelina Chochołowska Cave in the Tatra Mountains. Asterisks represent meteorological stations mentioned in the text: (a) Chochołowska Valley; (b) Kasprowy Wierch; (c) Hala Gąsienicowa; (d) Zakopane.
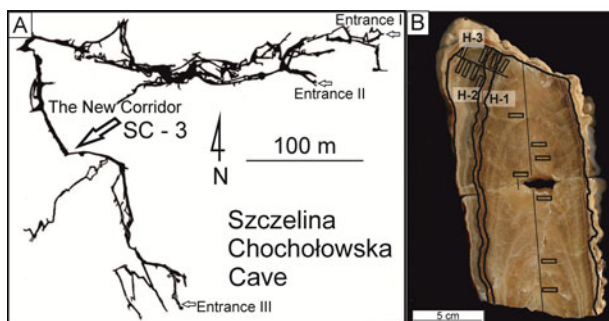

Figure 2. (color online) (A) Plan view of Szczelina Chochołowska Cave showing the location (a large open black arrow) where the stalagmite was collected (Luty 2013, modified); (B) the collected SC-3 stalagmite. Thin, straight black lines represent isotope tracks; black rectangles indicate U-Th dating; and thick black lines indicate hiatuses: H-1, H-2, and H-3.

precipitation during summer months than during winter. The ratio of winter (December–February) to summer (June–August) precipitation for the Chochołowska Valley is approximately 0.36 (Niedźwiedź, 1992).

The annual average $\delta^{18}O$ value of the monthly precipitation taken at Ornak Station, located at a similar altitude as the studied cave entrances, was $-11.26‰$ (Różański and Duliński, 1988). $\delta^{18}O$ values were also measured in surface outflows (springs, streams, discharges, and resurgences) and vadose seepage waters in the selected caves of the

western part of the Tatra Mountains (Różański and Duliński, 1988). During the period October 1983 to January 1986, the average $\delta^{18}O$ value of surface outflows was $-11.59 \pm 0.04‰$ (n = 43, variation ranged from $-12.05‰$ to $-11.25‰$) and that of vadose seepage waters collected in the Szczelina Chochołowska and Miętusia Caves was $-10.64 \pm 0.13‰$ (n = 19, variation ranged from $-11.65‰$ to $-9.8‰$; Różański and Duliński, 1988).

Stable isotope (O and C) analyses from limestone samples taken near the Szczelina Chochołowska entrances show average $\delta^{13}C$ and $\delta^{18}O$ values of approximately $0.47 \pm 0.13‰$ and $-2.79 \pm 0.52‰$, respectively.

MATERIALS AND METHODS

Material

The SC-3 stalagmite was collected in the New Corridor in Szczelina Chochołowska Cave (Fig. 2B). It is a 24.5-cm-high and 10-cm-wide fragment of a larger stalagmite with a broken base and top parts. Four macroscopically different parts, separated by hiatuses, can be distinguished. Those growth interruptions are underlined with layers of detrital material (Fig. 2B) and occur at 186 (H-1), 196.6 (H-2), and 230 mm (H-3) from the base of the sample. Successive stalagmite layers of calcite crystals differ in color, detrital material admixtures, porosity, and other calcite crystal features (Fig. 2B). The first type of calcite is dark yellow and indistinctly

laminated and contains a small admixture of detrital material. The second type of calcite is light brown with more visible calcite laminae and higher porosity. These two types are dominant in the older part of the stalagmite. The third type is dark brown and contains a greater admixture of detrital material. Changes in the growth axis direction occur in the upper part of the stalagmite, where hiatuses can also be observed (H-1 and H-2). At the time of the first hiatus, H-1, the SC-3 stalagmite growth axis changed (Fig. 2B). During the growth of this fragment, H-2 is visible but is not associated with a change in the growth direction. Finally, the stalagmite was broken (H-3) and covered with milky white layers of calcite that are indistinctly laminated and lack apparent porosity.

Methods

U-series dating and age–depth model construction

A series of calcite samples (approximately 200 mg each) were drilled along the lamina. The chemical separation of uranium and thorium from the carbonate matrix was performed at the U-series Laboratory of the Institute of Geological Sciences, Polish Academy of Sciences (IGS PAS; Warsaw, Poland) following the method described by Hellstrom (2003). Internal standards and blank samples were prepared and processed in parallel to all studied samples. The mass abundances of ^{236}U, ^{233}U, ^{234}U, ^{235}U, ^{229}Th, ^{230}Th, and ^{232}Th were measured with a double-focusing sector field Inductively Coupled Plasma (ICP) mass spectrometer (Element 2, Thermo Finnigan MAT) at the Institute of Geology of the Czech Academy of Sciences (Prague, Czech Republic). The measurement results were corrected for background counts and chemical blanks. The final results were reported as activity ratios. U-series ages were iteratively calculated from the $(^{230}Th/^{234}U)$ and $(^{234}U/^{238}U)$ activity ratios. All uncertainties, except uncertainties associated with decay constants, were taken into account when assessing age uncertainties using error propagation rules.

The ^{232}Th isotope is an indicator of contamination by thorium and/or uranium from detrital sources. For mass spectrometry, the threshold value of the $(^{230}Th/^{232}Th)_A$ for "clean samples" is commonly considered to be values of 200–300 (Hellstrom, 2006). However, common practice is to routinely correct all ages regardless of their measured $(^{230}Th/^{232}Th)_A$. The correction across the whole profile was made using a modified algorithm proposed by Hellstrom (2006), with adopted stratigraphical constraint using Monte Carlo simulation and the requirement that any axial sequence of true ages must exhibit a monotonic increase away from the outer surface. The main idea is to find the minimum possible contamination correction to set ages in stratigraphic order. Contrary to the algorithm proposed in Hellstrom (2006), the algorithm used (described for the first time and accessible on request) searches for the minimum values (between 0.01 and 20) of three initial activity ratios in contaminant: Th_0 $(^{230}Th/^{232}Th)_A$, U_1 $(^{234}U/^{232}Th)_A$, and U_2 $(^{238}U/^{232}Th)_A$ and estimates those values separately for each sample.

The whole procedure was repeated until the population of results for every sample (corrected ages and initial activity ratios in contaminant) in the profile was 1000. Based on this population, the corrected ages with 2σ errors were calculated for whole profile. The calculated corrected ages and possible lowest initial activity ratios of contaminant (Th_0, U_1, U_2) are presented in Table 1.

Based on the U-series dating results with 2σ errors, an age–depth model was created using the MOD-AGE algorithm (Hercman and Pawlak, 2012). The LOWESS technique was used to estimate age–depth relationships. The chosen SPAN value for the LOESS model was 0.38, representing the highest value of SPAN, which allowed the estimation of an age–depth model corresponding to all data points inside the 2σ confidence interval (Hercman and Pawlak, 2012).

Stable isotope analyses

The subsamples used for stable isotope analyses from SC-3 were drilled along its growth axis at approximately 1 mm increments, producing 225 samples. Additionally, three profiles were sampled along the growth layers at different distances from the SC-3 base, at 58, 134, and 172 mm, to perform the Hendy test (Hendy, 1971).

Analyses of the carbon and oxygen isotopic compositions ($\delta^{13}C$ and $\delta^{18}O$) were performed using a KIEL IV carbonate device (Thermo Scientific) coupled to a Delta Plus IRMS (Finnigan MAT) using the dual-inlet mode at the Stable Isotope Laboratory of the IGS PAS. The samples were prepared automatically according to the method described by McCrea (1950). Calcite samples were reacted with anhydrous orthophosphoric acid at 70°C. The results were normalized to two international standards, NBS 19 and IAEA CO 8, and were reported relative to the VPDB international standard. The reproducibility was checked by the measurement of two internal standards after every 12 samples. The analytical precision (1σ) was better than 0.03‰ and 0.08‰ for $\delta^{13}C$ and $\delta^{18}O$, respectively.

Petrography

Six thin sections covering the continuous profile of SC-3 were prepared to enable microscopic observations and the study of microscopic features, such as the appearance of calcite crystals, fabric type, discontinuities, and porosity. The microscopic observations were obtained using a Nikon Eclipse LV100POL microscope from the IGS PAS. The analysis and characterization of the speleothem fabrics were based mainly on the methodology proposed by Frisia (2015). As a result of the speleothem fabric analysis, it was possible to briefly characterize the environmental conditions that occurred during speleothem growth and create a fabric log for SC-3.

The mineralogical composition of the studied stalagmite was tested with X-ray diffractometry (XRD) in the Clay Mineral Laboratory of IGS PAS in Kraków using a Thermo Electron X'TRA diffractometer equipped with an automatic

Table 1. Results of the U-series dating of the stalagmite from Szczelina Chochołowska Cave.[a]

H[b] (mm)	U (ppm)	$(^{234}U/^{238}U)_A$[c]	$(^{230}Th/^{234}U)_A$[c]	$(^{230}Th/^{232}Th)_A$[c]	Age (ka)	Corrected age[d] (ka)	Initial[e] $(^{234}U/^{238}U)_A$[c]	Th_0	U_1	U_2
18 ± 1	0.779 ± 0.004	1.198 ± 0.004	0.997 ± 0.008	499 ± 4	320 ± 12	322 ± 13	1.487 ± 0.060	$0.016^{+0.023}_{-0.006}$	$0.016^{+0.021}_{-0.006}$	$0.016^{+0.021}_{-0.006}$
33 ± 1	0.834 ± 0.003	1.165 ± 0.002	0.989 ± 0.005	1716 ± 9	316 ± 7	317 ± 10	1.400 ± 0.044	$0.017^{+0.226}_{-0.007}$	$0.017^{+0.226}_{-0.007}$	$0.016^{+0.186}_{-0.006}$
85 ± 1	0.921 ± 0.003	1.161 ± 0.003	0.985 ± 0.007	5482 ± 40	310 ± 10	311 ± 11	1.384 ± 0.053	$0.016^{+0.021}_{-0.006}$	$0.016^{+0.019}_{-0.006}$	$0.016^{+0.021}_{-0.006}$
96 ± 1	0.895 ± 0.005	1.196 ± 0.003	0.970 ± 0.009	7190 ± 74	283 ± 11	297 ± 11	1.450 ± 0.039	$0.192^{+2.55}_{-0.182}$	$0.188^{+2.561}_{-0.178}$	$0.189^{+2.672}_{-0.179}$
112 ± 1	0.920 ± 0.003	1.162 ± 0.003	0.974 ± 0.006	4997 ± 34	295 ± 8	295 ± 10	1.369 ± 0.033	$0.019^{+0.804}_{-0.009}$	$0.018^{+0.817}_{-0.008}$	$0.019^{+1.112}_{-0.009}$
124 ± 1	1.116 ± 0.007	1.198 ± 0.003	0.978 ± 0.009	3514 ± 34	292 ± 12	293 ± 12	1.449 ± 0.035	$0.019^{+0.642}_{-0.009}$	$0.019^{+0.581}_{-0.009}$	$0.021^{+0.779}_{-0.011}$
155 ± 1	0.779 ± 0.003	1.195 ± 0.005	0.980 ± 0.006	7736 ± 37	294 ± 7	291 ± 8	1.440 ± 0.040	$0.019^{+1.071}_{-0.009}$	$0.018^{+1.042}_{-0.008}$	$0.019^{+0.972}_{-0.009}$
182 ± 1	1.038 ± 0.002	1.158 ± 0.002	0.970 ± 0.005	7842 ± 46	290 ± 7	289 ±7	1.354 ± 0.033	$0.017^{+0.437}_{-0.007}$	$0.017^{+0.518}_{-0.007}$	$0.017^{+0.671}_{-0.007}$
192 ± 1	0.610 ± 0.002	1.105 ± 0.002	0.944 ± 0.004	45 ± 1	273 ± 5	273 ± 6	1.225 ± 0.027	$0.018^{+0.008}_{-0.008}$	$0.018^{+0.011}_{-0.008}$	$0.019^{+0.011}_{-0.009}$
198.5 ± 1	1.000 ± 0.006	1.158 ± 0.002	0.936 ± 0.005	3345 ± 21	254 ± 5	253 ± 6	1.320 ± 0.032	$0.015^{+0.005}_{-0.005}$	$0.015^{+0.005}_{-0.005}$	$0.015^{+0.005}_{-0.005}$
200 ± 1	0.941 ± 0.002	1.100 ± 0.002	0.915 ± 0.008	9078 ± 90	242 ± 7	244 ± 7	1.198 ± 0.034	$0.015^{+0.006}_{-0.005}$	$0.015^{+0.007}_{-0.005}$	$0.015^{+0.006}_{-0.005}$
212 ± 1	1.143 ± 0.003	1.097 ± 0.002	0.908 ± 0.004	1299 ± 6	237 ± 3	237 ± 4	1.188 ± 0.020	$0.015^{+0.005}_{-0.005}$	$0.015^{+0.007}_{-0.005}$	$0.015^{+0.005}_{-0.005}$
219 ± 1	0.809 ± 0.005	1.162 ± 0.007	0.890 ± 0.008	180 ± 1	216 ± 5	217 ± 5	1.297 ± 0.025	$0.015^{+0.009}_{-0.005}$	$0.015^{+0.008}_{-0.005}$	$0.015^{+0.008}_{-0.005}$
223 ± 1	0.757 ± 0.002	1.119 ± 0.002	0.909 ± 0.004	203 ± 1	235 ± 4	216 ± 6	1.218 ± 0.034	$3.933^{+4.561}_{-3.923}$	$8.377^{+4.799}_{-8.367}$	$3.869^{+4.487}_{-3.859}$
225 ± 1	0.779 ± 0.005	1.142 ± 0.004	0.873 ± 0.011	619 ± 8	206 ± 7	205 ± 8	1.252 ± 0.049	$0.015^{+0.005}_{-0.005}$	$0.015^{+0.005}_{-0.005}$	$0.015^{+0.005}_{-0.005}$

[a]Calculations use the decay constants of Jaffey et al. (1971) (^{238}U), Cheng et al. (2013) (^{234}U and ^{230}Th), and Holden (1990) (^{232}Th). Ages do not include uncertainties associated with decay constants. Reported errors are equal to 2σ.
[b]H, distance from the base.
[c]Activity ratio.
[d]Corrected ages using the modified algorithm proposed by Hellstrom (2006) method described in more detail in the text.
[e]Calculated based on corrected $(^{234}U/^{238}U)_A$ and corrected age values.

sample changer and a specially adapted environmental chamber.

Trace element analyses

Trace element profiles were measured along the stalagmite growth axis in six thin 50 μm sections using the Laser Ablation Inductively Coupled Plasma Mass Spectrometry (LA-ICP-MS) method. For the measurements, an Analyte Excite Excimer laser ablation with a wavelength of 193 nm and an Element 2 (Thermo Finnigan) inductively coupled plasma mass spectrometer were used. The measurement was performed at the Institute of Geology of the Academy of Sciences in Prague, Czech Republic. The conditions for LA were a laser output of 50% with 10 Hz pulses, which achieved a fluency of 2.44 J/cm^2. The width of each line was 50 μm, and the laser speed during scans was 20 μm/s. The analysis of near-surface trace elements (Mg, Sr, Ba, Na, P, Si, Fe, Al, Cu, and U) was performed in one line at medium resolution. The measured intensities were normalized to the Ca content. Additional details of the LA-ICP-MS analytical procedure are described in Treble et al. (2003, 2005) and Desmarchelier et al. (2006).

RESULTS

Chronology of the SC-3 stalagmite

The results of the U-series dating are presented in Table 1. The reported errors of the SC-3 stalagmite data represent 2 standard deviations, and they vary from 1.5% to 3%. In almost all cases (except age 283 ka in the older and 237 ka in the younger part of the stalagmite), the ages corrected are within the error range of the uncorrected ages. The values of Th_0, U_1, and U_2 suggest negligible contamination for the majority of samples (Table 1). The light-brownish lamination appeared near the sampling point of the two samples with higher values of Th_0, U_1, and U_2 (Fig. 2B), probably indicating a higher detrital contamination.

The corrected U-series ages were used to generate the age–depth model for the studied speleothem. Based on the age–depth model of the SC-3 stalagmite (Fig. 3), the age of the oldest preserved layer in the stalagmite is estimated to be 327 ± 7 ka, and the growth of the older part of the stalagmite (below the H-1 hiatus) lasted continuously to approximately 289 ± 4 ka. The growth rate suggested by the model is rather stable at approximately 5 mm/ka, with only minor fluctuations.

The age–depth model for the youngest part of the stalagmite (above H-2) indicates that it was formed from ca. 250^{+10}_{-7} to 200^{+20}_{-17} ka ago (Fig. 3) with a much lower mean growth rate of approximately 0.6 mm/ka.

One U-series date, 273 ± 5 ka, was obtained from the part of the stalagmite between the H-1 and H-2 hiatuses (Fig. 2B). The growth of this part, which is composed of small, porous, sparse irregular calcite crystals with several micritic layers, was rather intermittent and took place during the MIS 8c
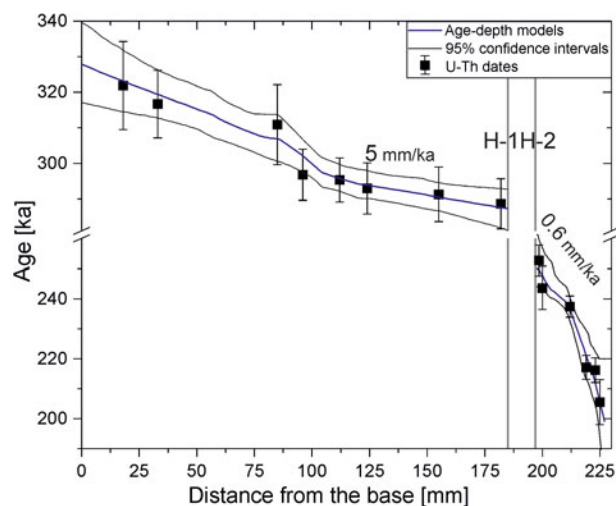

Figure 3. Age–depth model for the SC-3 stalagmite. The identified hiatuses, H-1 and H-2, are marked as gray lines. The numbers represent the growth rates for the different parts of the stalagmite. One U-Th date between hiatuses was omitted, because the model for this part of the stalagmite could not be built. (For interpretation of the references to color in this figure legend, the reader is referred to the web version of this article.)

stadial. Because only one date was obtained for that part and because of its possible discontinuous growth, an age–depth model could not be established, so the obtained proxy results are presented as the distance from the base scale with one benchmark.

Stable isotopes

The stable isotope records from the SC-3 speleothem are shown in Fig. 4B. The temporal resolution of the SC-3 stable isotope record is 0.2 ka for the older part of the stalagmite (below the H-1 hiatus), which grew continuously to approximately 289 ka, and 1.7 ka for the younger part (above the H-2 hiatus). The $\delta^{18}O$ values of SC-3 range from −7.97‰ ± 0.03 to −5.88‰ ± 0.02, and the $\delta^{13}C$ values range from −6.62‰ ± 0.02 to 2.19‰ ± 0.03 (Fig. 4B).

Petrography

Based on XRD of the macroscopically different parts of speleothems, it was confirmed that the SC-3 stalagmite is composed of calcite. A microscopic analysis of the appearance of the calcite crystals and an identification of the textural features of the studied material shows that most of the observed stalagmite is composed of elongated calcite crystals that are typical of the columnar fabric described in the work of Frisia (2015). The crystals range from 0.2 to 2.5 mm in width and 1 to approximately 3 mm in length. In most cases, they are perpendicular to the growth surface in each layer. Typically, the crystals are flush with each other; they are subparallel with one another and extinguish light at the same angle for the entire length of the crystals during microscopic observation.
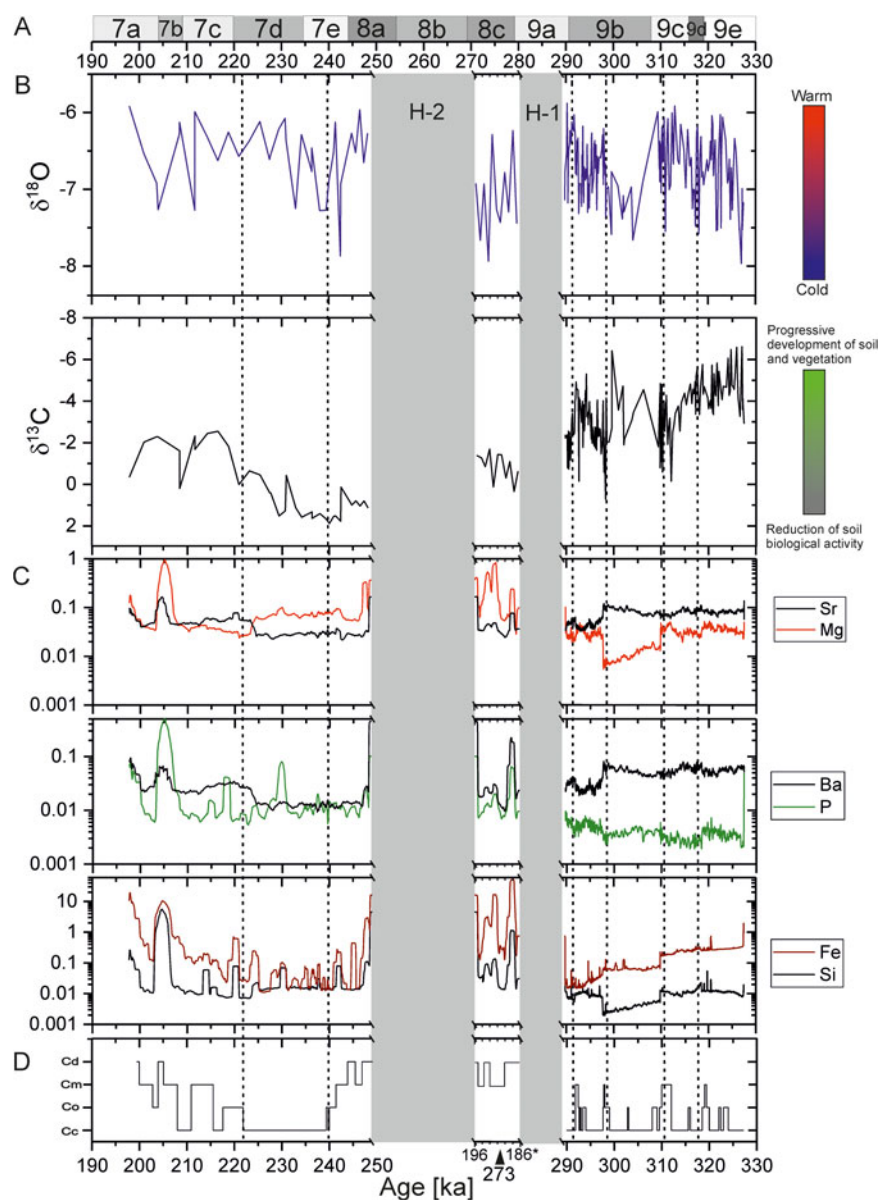
Figure 4. (color online) Combined data from the SC-3 record. (A) Marine isotopic substadials (Railsback et al., 2015); (B) oxygen and carbon stable isotope composition with marked hiatuses (gray rectangles) in SC-3; (C) trace element record; (D) fabric log. Cc, columnar compact fabric; Co, columnar open fabric; Cm, columnar microcrystalline fabric; Cd, dark layers with an abundance of detrital material, connected with hiatuses. *The section between hiatuses is presented as the distance from the base scale with one U-Th date as a benchmark. The dashed vertical lines represent the borders of distinct climatically different periods in our record.

The color of the crystals varies among clear, pale yellow, and brown. In the most commonly occurring type, columnar compact crystals form a compact aggregate, and the intercrystalline porosity is not discernible (Supplementary Fig. S1A and B). In the typical thin layers, characterized by the presence of linear inclusions or pores, columnar open crystals were identified (Supplementary Fig. S1A and B). In other parts of the stalagmite, the calcite crystallites have highly irregular boundaries; they are also characterized by inter- and intracrystalline microporosity and higher impurity content than in other parts (Supplementary Fig. S1C and D). These zones have the classical appearance of columnar microcrystalline fabric (Frisia, 2015). In those parts, a light-brownish lamination probably related to the periodic input of detrital/colloidal particulates also appears (Supplementary Fig. S1E and F). In the studied stalagmite, dark layers with an abundance of detrital material that are connected with hiatuses also occur (Supplementary Fig. S1G–I). Their occurrence indicates the presence of the most unstable stage, that is, corrosion and destruction conditions in the stalagmite, as well as the subsequent renucleation with geometric selection.

The results of the petrographic studies were based on fabric log construction (Fig. 4D). The older part of the stalagmite is dominated by columnar compact fabric with relatively narrow layers of columnar open fabric. Only in short periods, approximately 318, 312, and 298 ka, are parts of the SC-3 stalagmite

composed of smaller and irregularly growing crystallites, here classified as columnar microcrystalline fabric (Supplementary Fig. S1D). At approximately 293 ka, a change in the crystallization conditions is visible, and a relatively thin layer of the columnar microcrystalline fabric appears. The section between hiatuses in SC-3 is characterized by columnar microcrystalline fabric and the occurrence of small and irregular crystallites alternating with micritic layers and accumulations of detrital material (Supplementary Fig. S1D). After the H-2 hiatus, the transition to regular and larger crystallites with a dominant columnar compact fabric occurs at approximately 240 ka. The last period of SC-3 growth is also characterized by the dominance of the columnar microcrystalline fabric.

Trace elements

The trace element content along the profiles (normalized to the Ca content) is shown in Figure 4C, and the Pearson correlation values (*r*) between the different elements are reported in Table 2. The correlation between the near-surface trace elements changes slightly in different parts of the stalagmite, but the Sr and Mg contents are mostly moderately to strongly anticorrelated (with a minimum value of the correlation coefficient of −0.85 in SC-3 between 311 and 298 ka). Only the portions immediately preceding and following breaks in the growth of SC-3 are characterized by weak correlations (with a maximum of 0.32).

During the analysis of long-term changes in Sr content, a decrease at approximately 297 ka, relatively low values for the period after the H-2 hiatus until ca. 225 ka, and high values in the youngest part of the record can be observed. The Sr content in the profile (Fig. 4C), similar to the content of other trace elements, also increases near the growth hiatuses in the SC-3 stalagmite but is most likely associated with a higher detrital material supply in that period.

In the case of the Mg content (except in the zones associated with the hiatuses), the characteristic features are as follows: increases ca. 311 and 297 ka; lower values between ca. 310 and 297 ka; relatively high values in the period

Table 2. Pearson correlation coefficients (*r*) between trace element profiles measured in stalagmite SC-3.[a]

Trace element	Mg	Sr	P	Ba	Fe	Si
Mg	—	−0.596	0.059	−0.383	0.179	0.653
Sr		—	−0.696	0.846	0.578	−0.551
P			—	−0.033	−0.676	0.237
Ba				—	0.687	−0.431
Fe					—	0.801
Si						—

[a]Correlation coefficients (*r*) were calculated for the uninterrupted sections of the stalagmite, with the exception of the part between hiatuses and the parts immediately preceding and following breaks in the growth of SC-3. All reported Pearson correlation values (*r*) have *P* values < 0.001. Correlation is significant at the 0.05 level, so all results are statistically significant.

from approximately 248 to 225 ka; and low values in the subsequent period, except for a peak at approximately 205 ka (Fig. 4C).

The Ba content generally changes very similarly to the Sr content (Fig. 4C). The correlation coefficient between these elements reaches 0.95 in the older part of SC-3. The P content is generally characterized by slightly lower variability of values than in the case of other trace elements. The most prominent features are increased content near hiatuses and higher variability in the youngest layers of SC-3, after ca. 230 ka. The P and Ba contents are mostly in moderate anticorrelation (Table 2), except in periods connected with the growth hiatuses in SC-3, when these records react similarly.

The contents of Si and Fe change similarly throughout most of the profiles (Fig. 4C) and are usually moderately correlated (Table 2). However, the amplitude of changes in Fe content is higher than that observed in the changes in Si content. Higher Si and Fe contents can be observed in the youngest layers of SC-3 in particular, most likely connected with greater contamination from detrital material.

DISCUSSION

Factors controlling proxy records in the local environmental framework

The first requirement for using stable isotope records as a paleoclimatic proxy is deposition in the equilibrium state. SC-3 was collected in the deep part of the cave, with a stable microclimate representing the mean annual surface temperature of a region. The porosity in the stalagmite is low, and no significant alteration zones were observed. Similar speleothems generally tend to precipitate close to isotopic equilibrium (McDermott et al., 2006). Additionally, Hendy tests were performed, which are the classical tests employed to ascertain whether equilibrium conditions were achieved during calcite precipitation (Hendy and Wilson, 1968; Hendy, 1971).

Although Hendy's criteria have been challenged (Dorale and Liu, 2009), they can still indicate possible disequilibrium conditions during speleothem growth (e.g., Daëron et al. 2011; Kluge and Affek, 2012). The correlation coefficient between the $\delta^{18}O$ and $\delta^{13}C$ values along the axial profile was 0.21, and the results of Hendy's criteria suggest no disequilibrium for the SC-3 stalagmite (see Supplementary Fig. S2). Furthermore, a major part of the studied stalagmite (except the zone related to hiatuses) is composed of different types of columnar fabric, suggesting persistent water films, relatively constant flows, and the deposition of calcite from fluids at near-isotopic equilibrium conditions (Frisia et al., 2002; Frisia and Borsato, 2010). These petrographic studies support the idea that the growth of the SC-3 stalagmite occurred under conditions close to isotopic equilibrium.

Speleothems are very valuable material, especially because of their usefulness in paleoenvironmental research (e.g., McDermott et al., 2006; Lachniet, 2009; Fairchild and Baker, 2012). However, research based on speleothems

should be conducted comprehensively, using the gathered material to perform all possible studies, not just the most frequently performed tests (analysis of stable isotopes). An important benefit of a comprehensive analysis of all available data is the greater amount of climate-dependent records available for later interpretation. These analyses are invaluable, because many different factors can influence the stable isotope signal and other proxies, for example, circulation patterns, rainfall amount, temperature changes, cyclone intensity, vegetation cover, or even kinetic fractionation or evaporation (e.g., Lachniet, 2009; Dreybrodt and Scholz, 2011; Fairchild and Baker, 2012; Demény et al., 2017; Columbu et al., 2018).

The factors driving the oxygen isotope ratios in speleothems are numerous and vary on a spatial and temporal basis. In central and northern Europe, $\delta^{18}O$ variation is strongly positively related to the condensation temperature (+0.58‰/°C), whereas the influence of the rainfall amount on $\delta^{18}O$ is negligible (Różański et al., 1993). Additionally, the recently reported temperature effect for annual precipitation in Europe ranges from −0.11‰/1°C for Mediterranean sites (generally insignificant effects were observed at the coastal sites) and up to 0.75‰/1°C for continental locations; this relationship is expected to be preserved in the speleothem $\delta^{18}O$ record (Kern et al., 2019). Many aspects of atmospheric circulation during the analyzed period remain unknown. However, the reported mean annual precipitation relationships of +0.58‰/1°C and 0.75‰/1°C are well above the temperature dependence of water–calcite isotopic equilibrium fractionation (−0.177‰/1°C; Tremaine et al., 2011). Therefore, we consider the simplest scenario, in which the $\delta^{18}O$ variation observed in the SC-3 stalagmite primarily reflects a change in the mean annual temperature. That temperature dependence, which is often noted in records from central and northern Europe, is reflected in the $\delta^{18}O$ values, which are usually lower during colder periods and higher during warmer periods (e.g., Mangini et al., 2005; Spötl et al., 2006; Spötl and Mangini, 2007; Häuselmann et al., 2015; Moseley et al., 2015). Over short intervals, even if the $\delta^{18}O$ record is mainly controlled by the temperature, oxygen composition changes can respond more to variations in rainfall, but in these situations, the interpretation should be additionally supported by other proxies, such as the carbon isotopic composition and/or changes in the contents of trace elements, such as Mg, Sr, Ba, and P (e.g., Buhl et al., 2007).

The carbon isotope variations in the precipitated calcite are still not fully understood, but they most likely reflect climate-driven paleo-vegetation signals (e.g., McDermott et al., 2006). The $\delta^{13}C$ value in speleothems usually reflects the balance between isotopically light biogenic carbon derived from the soil CO_2 and heavier carbon dissolved from the limestone bedrock (e.g., Fairchild and Baker, 2012; Sharp, 2017; Zhang, 2018). It is accepted that in temperate zones, increasing $\delta^{13}C$ values in speleothems are related to a more significant contribution of ^{13}C-enriched carbon from bedrock dissolution and/or to a decrease in soil CO_2 productivity due to a reduction in rainfall and/or a cooler climate (e.g.,

Genty et al., 2001). A reduction in recharge can also produce degassing along the fracture paths, prior calcite precipitation, and longer rock–water interaction times, all resulting in higher $\delta^{13}C$ values in dripwater and speleothems (e.g., Fairchild et al., 2006; Fairchild and Baker, 2012). Finally, we interpreted the increase observed in the $\delta^{13}C$ proxy in the SC-3 stalagmite as a deterioration of climatic conditions, usually connected with cooler temperatures and/or a reduction in rainfall and consistently lower vegetation productivity.

Generally, analyzing trace element data is a challenging task, and without additional monitoring data, it is almost impossible to conclusively interpret the observed variations in trace element records. However, adopting a multiproxy approach enables the use of trace element records as support for building a more accurate interpretation of past hydrological variation (e.g., van Beynen et al. 2008; Fairchild and Treble, 2009). For example, many studies have demonstrated a convincing relationship between dripwater, Mg and Sr content in speleothems, and recorded rainfall (e.g., Tooth and Fairchild, 2003; Treble et al., 2003; McDonald et al., 2004). In the case of SC-3, we considered the correlation between high relative concentrations of Mg and Sr (especially connected with similar responses in $\delta^{13}C$) as an indicator of drier conditions possibly connected with the enhanced prior calcite precipitation (Fairchild and Treble, 2009; Johnson et al., 2006). In contrast, we used a lack of correlation between the Mg and Sr contents or even anticorrelation with generally higher Sr content, especially when associated with depleted $\delta^{13}C$ values, as a possible indication of warmer and wetter periods (Hellstrom and McCulloch, 2000; van Beynen et al., 2008). The Ba/Ca ratio can also be used as an effective paleohydrological indicator (e.g., Fairchild and Treble, 2009), and empirical studies have indicated that Ba concentrations tend to increase with the speleothem growth rate (e.g., Tesoriero and Pankow, 1996; Treble et al., 2003). We treated a higher Ba/Ca ratio as a possible indicator of wetter climatic conditions favorable for relatively fast growth in warm periods (e.g., Treble et al., 2003). The P content was also confirmed to be a reliable rainfall proxy that was dependent on the effects of climate on the rate of bioproduction, especially in regions where the soil P retention capacity is poor (e.g., Treble et al., 2003). We considered the observed increase in SC-3 speleothem P content to be a suggestion of environmental conditions favorable to vegetation productivity, with the higher water supply and infiltration flushing P from the soil (e.g., Huang et al., 2001; Treble et al., 2003). In the case of the Fe and Si contents, we considered the high Fe and Si contents to be potential indicators of wet periods when the total flux of detritus and infiltration were high (Hu et al., 2005; Fairchild and Treble, 2009).

Interpretation of climatic conditions based on data from the SC-3 stalagmite

The SC-3 stalagmite growing from MIS 9e to MIS 7 covers a very interesting period of the transition from one of the

warmest interglaciations (MIS 9, especially MIS 9e) through MIS 8, which appears to be a weak glaciation in many records (particularly benthic δ^{18}O; Lisiecki and Raymo, 2005), to the MIS 7 interglaciation, which generally exhibits widespread weakness (e.g., Lang and Wolff, 2011; Berger et al., 2015). The multiproxy data obtained allow for analysis of this period with higher resolution and the estimation of local impacts based upon observed global climatic variability. This first period of speleothem growth, from MIS 9e to MIS 9c, took place in favorable climatic conditions (warm and humid) with a high and stable water supply, suggested by the high δ^{18}O values, low δ^{13}C values, and the occurrence of columnar compact and columnar open fabrics (Fig. 4B and D). Only a relatively short, slightly colder period, evidenced by a small decrease in δ^{18}O values and a minor increase in δ^{13}C values (Fig. 4B), correlated with MIS 9d, can be noted. Then, at the MIS 9c/MIS 9b transition, the step changes observed in several proxies, that is, short peaks in δ^{18}O and δ^{13}C values and the relatively high content of Mg, suggest the occurrence of a drier episode but may also be connected with the shift in the sampling path made to avoid the physical break in the sample (Fig. 2). MIS 9b in the Tatra Mountains was a period characterized by higher variability in climatic conditions. In the first part of the MIS 9b transition, the lower δ^{18}O values suggest decreasing temperatures (Fig. 4B) but still relatively wet climatic conditions, with no signs of prior calcite precipitation indicated by relatively high Sr and Ba contents or strong anti-correlation between the Mg and Sr contents (Fig. 4C). Then, a strong hydrological condition change near the cave, possibly related to a strong infiltration event causing massive flushing of detritus, can be inferred based on an increase in both the δ^{18}O and δ^{13}C values, the occurrence of columnar to microcrystalline fabric connected with changes in the water supply, and rapid changes in the trace element contents (Fig. 4B–D). The last part of MIS 9b is connected with stable growth conditions but with rather low temperatures, as evidenced by a decrease in the δ^{18}O value in SC-3 (Fig. 4B). This period was also characterized by higher precipitation and greater vegetation development, as indicated by the lower δ^{13}C values and the relatively high P and Mg (Fig. 4B and C). In the last period of the MIS 9b/MIS 9a transition before the H-1 hiatus, short peaks in the δ^{18}O and δ^{13}C values and rapid changes in the trace element content suggest a reduction in precipitation that could be the main cause of the SC-3 growth cessation ca. 288 ka.

For the subsequent growth period in MIS 8, due to breaks in SC-3 growth and the impossibility of building the age–depth model for that section, detailed paleoclimatic conditions cannot be inferred on a temporal basis. All data obtained from that part give us only some rough suggestions about rather low temperatures, indicated by relatively low and variable δ^{18}O values and high δ^{13}C values (Fig. 4B) and the occurrence of periods with intensive rainfall, a periodically higher water supply, and a high infiltration rate (Fig. 4B–D) in the Tatra Mountains during MIS 8.

The first part of SC-3 growth after the H-2 hiatus can be interpreted as an indication of higher temperatures, suggested by the high values of δ^{18}O, as well as an effect of generally diminished rainfall, indicated by high trace element content and/or the occurrence of columnar microcrystalline fabric (Fig. 4C and D). The next period of growth until MIS 7d was probably connected with variable temperatures but relatively stable water supply and still poorly developed vegetation, evidenced by variable δ^{18}O values, relatively high δ^{13}C values, small fluctuations in trace element contents, and the occurrence of columnar compact fabric (Fig. 4B–D). In late MIS 7, the proxy record indicates not only the beginning of vegetation development, as suggested by an increase in δ^{13}C values (Fig. 4B), but also strong hydrological changes, especially from MIS 7b, interpreted based on stronger fluctuations in all trace element contents and the occurrence of the columnar microcrystalline fabric (Fig. 4C and D), which could cause instability in dripwater supply and/or instability in the bedrock or the ceiling. The SC-3 record stopped in MIS 7a, and the youngest part of the stalagmite was most likely destroyed at H-3.

The obtained SC-3 data in the context of other U-Th–dated records

The obtained speleothem record is one of very few long-term sources of information reported so far based on speleothem studies concerning climatic changes during glacial conditions in MIS 8 (e.g., Hercman et al., 1997, 1998; Hercman, 2000; Plagnes et al., 2002; Drysdale et al., 2004; Spötl and Mangini, 2007; Columbu et al., 2018; Regattieri et al., 2018). The records obtained from the Tatra Mountains indicate that the best climatic conditions for speleothem growth occurred in MIS 9e, and, for example, a trend of increasing δ^{13}C values suggest subsequent gradually decreasing soil/vegetation activity as the climate cooled and the ice volume increased throughout MIS 9 (Fig. 5C). MIS 8 in the Tatra Mountains is associated with cold temperatures and conditions that were worse for vegetation development but enabled intermittent speleothem growth. The interpreted climatic conditions during MIS 7 indicate that this interglaciation was periodically drier than and not as warm as MIS 9. Such characteristics of the marine isotopic stages correspond relatively well with the variability observed in global records, for example, summer insolation data (Huybers, 2006; Fig. 5D) and stacked benthic oxygen isotope curves (Lisiecki and Raymo, 2005; Fig. 5E).

Several long-term speleothem paleoclimatic records reaching the MIS 9 period in Europe have been published (Fig. 5F–H). The records include the Macedonian stalagmite OH2 collected in a cave near Lake Ohrid (Regattieri et al., 2018), an alpine record based on the GG1 stalagmite from the Piani Eterni karst system (Columbu et al., 2018), the Italian speleothem CC1 collected in Antro del Corchia Cave in the Alpi Apuane massif (Drysdale et al., 2004), and the last record from the SPA 4 flowstone from the alpine Spannagel Cave (Spötl and Mangini, 2007). However, the last stalagmite record was published without a proper chronology and relied
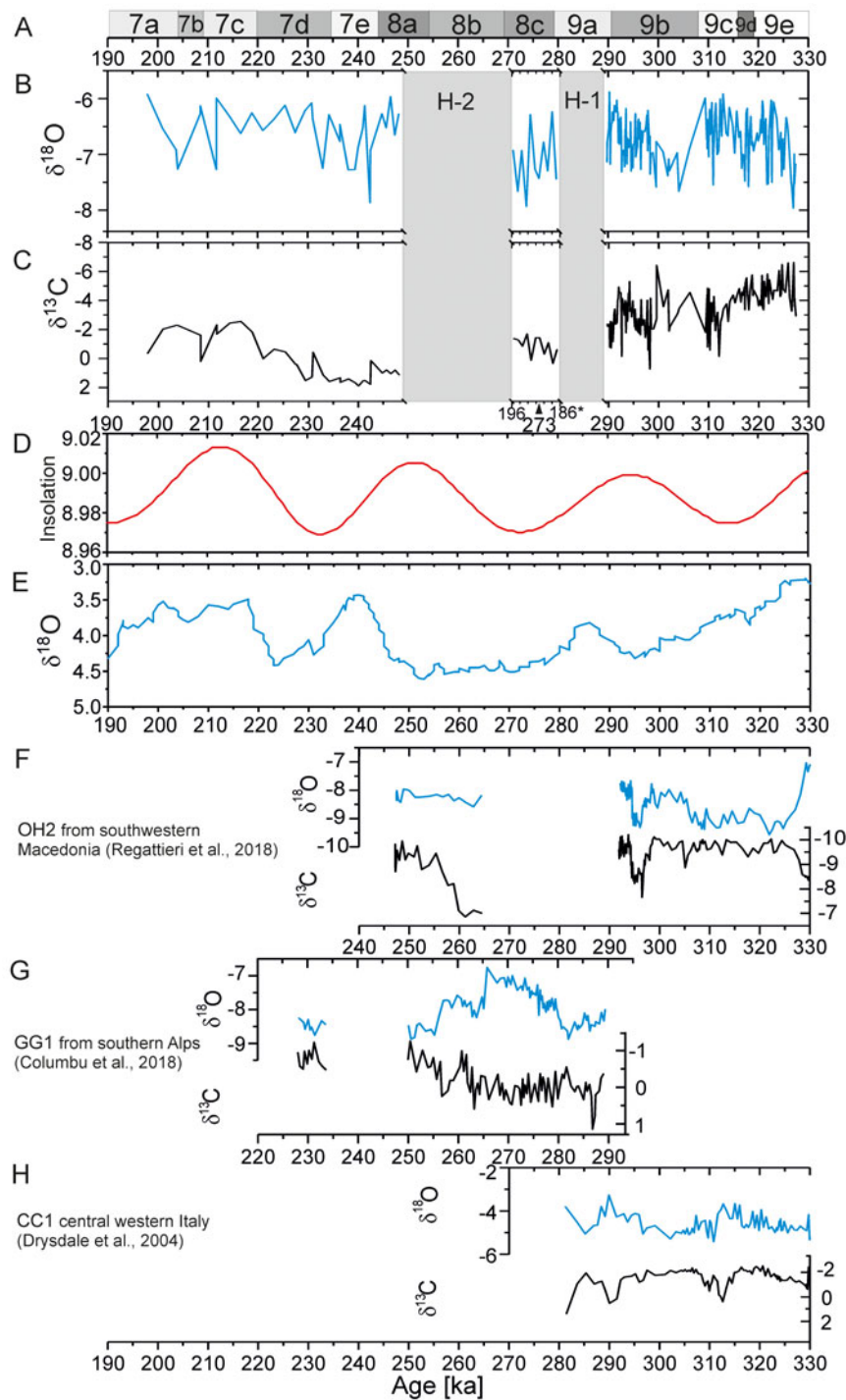
Figure 5. (color online) The comparison of the $\delta^{18}O$ and $\delta^{13}C$ records from SC-3 with global data and selected speleothems from Europe. (A) Marine isotopic substadials (Railsback et al., 2015); (B and C) oxygen and carbon stable isotope composition with marked hiatuses (gray rectangles) in SC-3; (D) integrated summer insolation at 50°N (Huybers, 2006); (E) stacked benthic oxygen isotope curve (Lisiecki and Raymo, 2005); (F) oxygen and carbon stable isotope composition from southwestern Macedonia (Regattieri et al., 2018); (G) oxygen and carbon stable isotope composition from southern Alps (Columbu et al., 2018); (H) oxygen and carbon stable isotope composition from central western Italy (Drysdale et al., 2004).

on only a few U-series benchmarks. The main phases of growth of SC-3, OH2, and CC1 speleothems took place in similar time periods, and hiatuses H-1 and H-2 in SC-3 are coincident with the growth break in the Macedonian OH2 stalagmite (Fig. 5F–H). The growth of the alpine GG1 stalagmite started later and corresponds with the end of the growth of the OH2 stalagmite and with the H-1 hiatus in the SC-3 stalagmite (Fig. 5F–H).

The $\delta^{18}O$ values in the southern alpine speleothem GG1 are mostly influenced by the amount of rainfall (Columbu et al., 2018) and are thus similar to those of the Macedonian OH2 stalagmite, in which oxygen isotope variations are also interpreted as being strongly related to variations in the rainfall amount (Regattieri et al., 2018). On the other hand, CC1 records show strong similarities to regional sea-surface temperature records (Drysdale et al., 2004). Therefore, the authors suggested that the main factor that influenced the $\delta^{18}O$ values was the temperature. Additionally, the $\delta^{18}O$ values in the SPA 4 record are mostly modeled by the atmospheric temperature signal (Spötl and Mangini, 2007). In the Tatra Mountains speleothem records, the oxygen isotope variations seem to be mainly dependent on temperature changes. The cessations of growth in OH2 and the growth break in the CC1 record were interpreted by the authors as being connected to subzero temperatures and/or ice above the caves at the time and to decreased rainfall during the glacial period (Drysdale et al., 2004, Regattieri et al., 2018). In the case of the GG1 record, growth breaks during the interglacial period were interpreted as a result of floods and water migration creating epiphreatic paths filled with fine-grained sediments (Columbu et al., 2018). Speleothem growth breaks have also been reported during full glacial periods (Columbu et al., 2018). The first recorded hiatus in SC-3 was most likely associated with a reduction in precipitation, and H-2 could be an effect of strong hydrological changes in the Tatra Mountains.

The $\delta^{13}C$ records from all speleothems in this comparison are related to the different contributions of ^{13}C-depleted organic CO_2 from the soil and of ^{13}C-enriched CO_2 from bedrock dissolution and/or to a decrease in soil CO_2 productivity due to a reduction in rainfall and/or a cooler climate. Similar to those in the SC-3 record, the $\delta^{13}C$ values in the SPA 4, CC1, and GG1 speleothems approach high levels (even above 0.0‰), reflecting the minimal influence of pedogenic $\delta^{13}C$ values. Two possible reasons for this finding can be proposed. The first could be related to climatic conditions, in which high $\delta^{13}C$ values suggest rather harsh, cold climatic conditions that did not allow intensive vegetation development during the growth of those speleothems. The second could be related to differences in the local morphology, for example, steep slopes preventing the development of a thick soil layer or fast water circulation that allowed no time for biogenic CO_2 saturation. The much lower $\delta^{13}C$ values in the Macedonian stalagmite suggest that the soil above the cave was relatively well developed during almost the entire period of stalagmite growth.

A brief characterization of climatic evolution supported by comparison with other records

In summary, the MIS 9 interglacial period in most speleothem records, including SC-3, was a time of major growth and a dominant warm and wet climate until MIS 9a, which was characterized by reduced precipitation. Similar warm and humid conditions during MIS 9 were also reported from the southeastern Essex channel deposits (Roe et al., 2009; I in Fig. 1A), pollen records from northern Germany (Urban, 2007; II in Fig. 1A) and Lake Ohrid (Sadori et al., 2016; III in Fig. 1A). The best climatic conditions for speleothem growth in the SC-3 record can also be correlated with the main forest phases visible in pollen records (e.g., Fletcher et al., 2013; IV in Fig. 1A; Sadori et al., 2016). The end of the main growth phase of the SC-3 stalagmite is actually simultaneous with the change from warmer and wetter to cooler and drier conditions observed in the pollen record from Lake Ohrid and similar to growth breaks in the CC1 (Drysdale et al., 2004) and OH2 (Regattieri et al., 2018) speleothems, which may be indicative of similarities in the climatic fluctuations observed in Poland and southern Europe.

MIS 8 was a period associated with relatively cold temperatures and worse conditions for vegetation development, but at least in some periods, speleothem growth was not prevented: that is, the growth of GG1 during MIS 8c-MIS 8b or the short SC-3 growth phase in MIS 8c. Most likely there was no strong influence of glaciers in the Tatra Mountains at that time, and the hiatuses were associated with extreme hydrologic events, such as strong rainfall leading to mountain slope deformation (e.g., Szczygieł et al., 2019). The characteristics of MIS 8 recorded in the Tatra Mountains speleothem indicate a rather different course for this glaciation than has been recorded in the Mediterranean region, where it was associated with extended plateau-like structures with low-amplitude variability and mainly the presence of regional grasslands, which is typical for glacial periods in southeastern Europe (e.g., Fletcher et al., 2013; Sadori et al., 2016). The observed stable isotope variations in the SC-3 stalagmite during MIS 8 are possibly connected with local climatic factors and related to changes in the average temperatures and/or precipitation, similar to speleothem records from the Alps (e.g., Spötl and Mangini, 2007; Columbu et al., 2018).

MIS 7, based on all presented speleothem records, was drier and not as warm as the previous MIS 9 interglaciation. The GG1 speleothems had only a short growth phase, and in the cases of the OH2, CC1, and SPA 4 speleothems, there were no growth phases during the entirety of MIS 7. The rather long growth period during MIS 7 in the Tatra Mountains is distinctive, but the slow growth rate and recorded proxies, mainly trace elements and petrographic features, clearly indicate worse climatic conditions for speleothem growth, with a less stable water supply than during the previous MIS 9 interglaciation. MIS 7 also had vegetation behavior quite different from MIS 9, as seen in pollen records (Urban, 2007; Sadori et al., 2016); the MIS 7 interglaciation was connected with very high forest variability, which was sometimes even interrupted by herbaceous expansions. On the other hand, despite the conditions of the relatively weak interglaciation, which are discussed more widely in Berger et al. (2015), the climate was warm and humid enough to enable speleothem growth in Poland; this is similar to findings from the Alps region, where long periods of speleothem growth during this period were also noted (e.g., Spötl and Mangini, 2007; Spötl et al., 2008).

CONCLUSIONS

In comparison with those of other studied MIS 9–7 European speleothems, the record obtained from the Tatra Mountains speleothem is distinguished mainly by longer uninterrupted periods of growth covering the major part of MIS 9 and MIS 7, but also a by short episode in the MIS 8 glaciation.

The obtained paleoclimatic reconstruction implies that the best climatic conditions for speleothem growth under warm and wet conditions occurred during periods in MIS 9e and MIS 9c, and several short periods of unstable hydrological conditions and/or slightly reduced precipitation were also apparent. The first recorded hiatus at the MIS 9/MIS 8 transition was most likely connected with a reduction in precipitation. The reasons for the SC-3 growth stoppage in MIS 8 (H-2) cannot be unambiguously stated, but the obtained proxies indicate the occurrence of extreme hydrologic events in the Tatra Mountains, which could have caused a massive flushing of detritus and impaired speleothem growth.

The recorded phase of growth during the MIS 8 glaciation suggests that it was a relatively mild glaciation in the Tatra Mountains, with no strong influence of glaciers or freezing temperatures to prevent speleothem growth.

The obtained SC-3 record indicates worsened climatic conditions for speleothem growth during MIS 7, which was periodically drier and not as warm as MIS 9, yet still sufficient to sustain a long period of speleothem growth.

The comparison of the Tatra Mountains records with other European records revealed similarities, which suggests that the climatic variability recorded in the speleothems from the Tatra Mountains can be linked to extraregional climatic changes during both interglacial and glacial periods. The almost simultaneous climatic shifts observed in the SC-3 record during MIS 9 indicate that the climate in the Tatra Mountains could also have been influenced by the Mediterranean climate. On the other hand, the revealed differences, especially in MIS 8 and MIS 7, between our record and the Mediterranean records suggest the dominant role of the Atlantic climate in the Tatra Mountains, similar to its role in western Europe or the northern Alps.

This work provides the northernmost paleoclimatic record for the whole Carpathian range and one of the very few records from those periods worldwide. The results of this work also further affirm that speleothems are fundamental tools for understanding paleoclimate and show great potential for such studies in the middle Pleistocene, especially in central Europe, which is poorly represented in such studies.

ACKNOWLEDGMENTS

SUPPLEMENTARY MATERIAL

The supplementary material for this article can be found at https://doi.org/10.1017/qua.2020.69

REFERENCES

Ayalon, A., Bar-Matthews, M., Kaufman, A., 2002. Climatic conditions during Marine Isotope Stage 6 in the eastern Mediterranean region from the isotopic composition of speleothems of Soreq Cave, Israel. *Geology* 30, 303–306.

Bar-Matthews, M., Ayalon, A., Gilmour, M., 2003. Sea–land oxygen isotopic relationships from planktonic foraminifera and speleothems in the eastern Mediterranean region and their implication for paleorainfall during interglacial intervals. *Geochimica et Cosmochimica Acta* 67, 3181–3199.

Barczyk, G., 2004. Recent results of the dye tracer tests of Chochołowskie Vaucluse Spring karst system (western Tatra Mts.). *Acta Geologica Polonica, Warszawa* 54, 169–177.

Bard, E., Delaygue, G., Rostek, F., Antonioli, F., Silenzi, S., Schrag, D.P., 2002. Hydrological conditions over the western Mediterranean basin during the deposition of the cold Sapropel 6 (ca 175 kyr BP). *Earth and Planetary Science Letters* 202, 481–494.

Berger, A., Crucifix, M., Hodell, D.A., Mangili, C., McManus, J.F., Otto-Bliesner, B., Pol, K., et al., 2015. Interglacials of the last 800,000 years. *Reviews of Geophysics* 54, 162–219.

Borówka, R.K., Kostrzewski, A., Zwolinski, Z., 1985. Cave sediments from the Chocholowska Valley (the Tatra Mountains, Poland): interpretation of sequences and depositional processes. *Quaestiones Geographicae* 9, 5–24.

Buhl, D., Immenhauser, A., Smeulders, G., Kabiri, L., Richter, D.K., 2007. Time series δ^{26}Mg analysis in speleothem calcite: kinetic versus equilibrium fractionation, comparison with other proxies and implications for palaeoclimate research. *Chemical Geology* 244, 715–729.

Cheng, H., Edwards, R.L., Shen, C.C., Polyak, V.J., Asmerom, Y., Woodhead, J., Hellstrom, J., et al.., 2013. Improvements in ^{230}Th dating, ^{230}Th and ^{234}U half-life values, and U-Th isotopic measurements by multi-collector inductively coupled plasma mass spectrometry. *Earth and Planetary Science Letters* 371–372, 82–91.

Columbu, A., Sauro, F., Lundberg, J., Drysdale, R.N., Waele, J.D., 2018. Palaeoenvironmental changes recorded by speleothems of the southern Alps (Piani Eterni, Belluno, Italy) during four interglacial to glacial climate transitions. *Quaternary Science Reviews* 197, 319–335.

Daëron, M., Guo, W., Eiler, J., Genty, K., Blamart, D., Boch, R., Drysdale, R. N., Maire, R., Wainer, K., Zanchetta, G., 2011. ^{13}C^{18}O clumping in speleothems: observations from natural cave and precipitation experiments. *Geochimica et Cosmochimica Acta* 75, 3303–3317.

Demény, A., Kern, Z., Czuppon, G., Németh, A., Leél-Őssy, S., Siklósy, Z., Haszpra, L., 2017. Stable isotope compositions of speleothems from the last interglacial–spatial patterns of climate fluctuations in Europe. *Quaternary Science Reviews* 161, 68–80.

Desmarchelier, J.M., Hellstrom, J.C., McCulloch, M., 2006. Rapid trace element analysis of speleothems by ELA-ICP-MS. *Chemical Geology* 231, 102–117.

Dorale, J.A., Liu, Z., 2009. Limitations of Hendy test criteria in judging the paleoclimatic suitability of speleothems and the need for replication. *Journal of Cave and Karst Studies* 71, 73–80.

Dreybrodt, W., Scholz, D., 2011. Climatic dependence of stable carbon and oxygen isotope signals recorded in speleothems: from soil water to speleothem calcite. *Geochimica et Cosmochimica Acta* 75, 734–752.

Drysdale, R.N., Zanchetta, G., Hellstrom, J.C., Fallick, A.E., Zhao, J.X., Isola, I., Bruschi, G., 2004. Palaeoclimatic implications of the growth history and stable isotope (δ^{18}O and δ^{13}C) geochemistry of a Middle to Late Pleistocene stalagmite from central-western Italy. *Earth and Planetary Science Letters* 227, 215–229.

Fairchild, I.J., Baker, A., 2012. *Speleothem Science. From Process to Past Environments*. Wiley, Oxford.

Fairchild, I.J., Smith, C.L., Baker, A., Fuller, L., Spötl, C., Mattey, D., McDermott, F., 2006. Modification and preservation of environmental signals in speleothems. *Earth-Science Reviews* 75, 105–153.

Fairchild, I.J., Treble, P.C., 2009. Trace elements in speleothems as recorders of environmental change. *Quaternary Science Reviews* 28, 449–468.

Fletcher, W.J., Muller, U.C., Koutsodendris, A., Christanis, K., Pross, J., 2013. A centennial-scale record of vegetation and climate variability from 312 to 240 ka (Marine Isotope Stages 9c-a, 8 and 7e) from Tenaghi Philippon, NE Greece. *Quaternary Science Reviews* 78, 108–125.

Frisia, S., 2015. Microstratigraphic logging of calcite fabrics in speleothems as tool for palaeoclimatic studies. *International Journal of Speleology* 44, 1–16.

Frisia, S., Borsato, A., 2010. Karst. In: Alonso-Zarza, A.M., Tanner, A. (Eds.), Carbonates in Continental Settings. *Developments in Sedimentology 61*. Elsevier, New York, pp. 269–318.

Frisia, S., Borsato, A., Fairchild, I.J., McDermott, F., Selmo, E.M., 2002. Aragonite-calcite relationships in speleothems (Grotte De Clamouse, France): environment, fabrics, and carbonate geochemistry. *Journal of Sedimentary Research,* 72, 687–699.

Genty, D., Baker, A., Vokal, B., 2001. Intra-and inter-annual growth rate of modern stalagmites. *Chemical Geology* 176, 191–212.

Gradziński, M., Dulinski, M., Hercman, H., Górny, A., Przybyszowski, S., 2012. Peculiar calcite speleothems filling fissures in calcareous sand stones and their palaeohydrological and palaeoclimatic significance: an example from the Polish Carpathians. *Geological Quarterly* 56, 711–732.

Gradziński, M., Hercman, H., Kicińska, D., Barczyk, G., Bella P., Holúbek, P., 2009. Karst in the Tatra Mountains—developments of knowledge in the last thirty years. [In Polish.] *Przegląd Geologiczny* 57, 674–684.

Häuselmann, A.D., Fleitmann, D., Cheng, H., Tabersky, D., Günther, D., Edwards, R.L., 2015. Timing and nature of the penultimate deglaciation in a high alpine stalagmite from Switzerland. *Quaternary Science Reviews* 126, 264–275.

Hellstrom, J., 2003. Rapid and accurate U/Th dating using parallel ion-counting multicollector ICP-MS. *Journal of Analytical Atomic Spectrometry* 18, 135–1346.

Hellstrom, J., 2006. U–Th dating of speleothems with high initial ^{230}Th using stratigraphical constraint. *Quaternary Geochronology* 1, 289–295.

Hellstrom, J.C., McCulloch, M.T., 2000. Multi-proxy constraints on the climatic significance of trace element records from a New Zealand speleothem. *Earth and Planetary Science Letters* 179, 287–297.

Hendy, C.H., 1971. The isotopic geochemistry of speleothems—I. The calculation of the effects of different modes of formation on the isotopic composition of speleothems and their applicability as palaeoclimatic indicators. *Geochimica et Cosmochimica Acta* 35, 801–824.

Hendy, C.H., Wilson, T.A., 1968. Palaeoclimatic data from speleothems. *Nature* 219, 48–51.

Hercman, H., 2000. Reconstruction of palaeoclimatic changes in central Europe between 10 and 200 thousand years BP, based on analysis of growth frequency of speleothems. *Studia Quaternaria* 17, 35–70.

Hercman, H., Bella, P., Głazek, J., Gradziński, M., Lauritzen, S.E., Løvlie, R., 1997. Uranium-series of speleothems from Demänova Ice Cave: a step to age estimation of the Demänova Cave System. *Annales Societatis Geologorum Poloniae* 67, 439–450.

Hercman, H., Gradziński, M., Bella, P., 2008. Evolution of Brestovská Cave based on U-series dating of speleothems. *Geochronometria* 32, 1–12.

Hercman, H., Nowicki, T., Lauritzen, S.E., 1998. Development of Szczelina Chochołowska cave (Western Tatra Mts.), based on uranium-series dating of speleothems. *Studia Geologica Polonica* 113, 85–103.

Hercman, H., Pawlak, J., 2012. MOD-AGE: an age-depth model construction algorithm. *Quaternary Geochronology* 12, 1–10.

Holden, E.N., 1990. Total half-lives for selected nuclides. *Pure and Applied Chemistry* 62, 941–958.

Huang, Y., Fairchild, I.J., Borsato, A., Frisia, S., Cassidy, N.J., McDermott, F., Hawkesworth, C.J., 2001. Seasonal variations in Sr, Mg and P in modern speleothems (Grotta di Ernesto, Italy). *Chemical Geology* 175, 429–448.

Hu, C., Huang, J., Fang, N., Xie, S., Henderson, G.M., Cai, Y., 2005. Adsorbed silica in stalagmite carbonate and its relationship to past rainfall. *Geochimica et Cosmochimica Acta* 69, 2285–2292.

Huybers, P., 2006. Early Pleistocene glacial cycles and the integrated summer insolation forcing. *Science* 313, 508–511.

Jaffey, A.H., Flynn, K.F., Glendenin, L.E., Bentley, W.C., Essling, A.M., 1971. Precision measurement of half-lives and specific activities of ^{235}U and ^{238}U. *Physical Review* C4, 1889–1906.

Johnson, K.R., Hu, C., Belshaw, N.S., Henderson, G.M., 2006. Seasonal trace-element and stable-isotope variations in a Chinese speleothem: the potential for high-resolution paleomonsoon reconstruction. *Earth and Planetary Science Letters* 244, 394–407.

Jurewicz, E., 2005. Geodynamic evolution of the Tatra Mts. and the Pieniny Klippen Belt (western Carpathians): problems and comments. *Acta Geologica Polonica* 3, 295–338.

Kern, Z., Demény, A., Perşoiu, A., Hatvani, I.G., 2019. Speleothem stable isotope records from eastern Europe & Turkey. *Quaternary* 2, 31.

Kicińska, D., Hercman, H., Najdek, K., 2017. Evolution of the Bystrej Valley caves (Tatra Mts, Poland) based on corrosive forms, clastic deposits and U-series speleothem dating. *Annales Societatis Geologorum Poloniae* 87, 101–119.

Kłapyta, P., Zasadni, J., 2018. Research history on the Tatra Mountains glaciations. *Studia Geomorphologica Carpatho-Balcanica* 51, 43–85.

Kluge, T., Affek, H.P., 2012. Quantifying kinetic fractionation in Bunker Cave speleothems using $\Delta47$. *Quaternary Science Reviews* 49, 82–94.

Lachniet, M.S., 2009. Climatic and environmental controls on speleothem oxygen-isotope values. *Quaternary Science Reviews* 28, 412–432.

Lang, N., Wolff, E.W., 2011. Interglacial and glacial variability from the last 800 ka in marine, ice and terrestrial archives. *Climate of the Past* 7, 361–380.

Lisiecki, L.E., Raymo, M.E., 2005. A Pliocene–Pleistocene stack of 57 globally distributed benthic δ^{18}O records. *Paleoceanography* 20, PA1003.

Luterbacher, J., Xoplaki, E., Küttel, M., Zorita, E., González-Rouco, F.J., Jones, P.D., Stössel, M., *et al.*, 2010. Climate change in Poland in the past centuries and its relationship to European climate: evidence from reconstructions and coupled climate models. In: Przybylak, R, Majorowicz, J, Brázdil, R. (Eds.), *The Polish Climate in the European Context: An Historical Overview.* Springer, Berlin, pp. 3–39.

Luty, I., 2013. Szczelina Chochołowska (accessed September 19, 2009). http://geoportal.pgi.gov.pl/portal/page/portal/jaskinie_polski.

Makos, M., Dzierżek, J., Nitychoruk, J., Zreda, M., 2014. Timing of glacier advances and climate in the High Tatra Mountains (western Carpathians) during the Last Glacial Maximum. *Quaternary Research* 82, 1–13.

Mangini, A., Spötl, C., Verdes, P., 2005. Reconstruction of temperature in the central Alps during the past 2000 yr from a $\delta^{18}O$ stalagmite record. *Earth and Planetary Science Letters* 235, 741–751.

Marks, L., 2011. Quaternary glaciations in Poland. In: Ehlers, J., Gibbard, P.L., Hughes, P.D. (Eds.), *Quaternary Glaciations—Extent and Chronology, A Closer Look.* Developments in Quaternary Science 15. Elsevier, Amsterdam, pp. 299–303.

McCrea, J.M., 1950. On the isotopic chemistry of carbonates and a paleotemperature scale. *Journal of Chemical Physics* 18, 6, 849–857.

McDermott, F., Schwarcz, H.P., Rowe, P.J., 2006. Isotopes in speleothems. In: Leng, M. (Eds.), *Isotopes in Palaeoenvironmental Research* 10. Springer, Dordrecht, pp. 185–226.

McDonald, J., Drysdale, R., Hill, D., 2004. The 2002–2003 El Niñõ recorded in Australian cave drip waters: implications for reconstructing rainfall histories using stalagmites. *Geophysical Research Letters* 31. http://dx.doi.org/10.1029/2004GL020859.

Moseley, G.E., Spötl, C., Cheng, H., Boch, R., Min, A., Edwards, R.L., 2015. Termination-II interstadial/stadial climate change recorded in two stalagmites from the north European Alps. *Quaternary Science Reviews* 127, 229–239.

Niedźwiedź, T., 1992. Climate of the Tatra Mountains. *Mountain Research and Development* 12, 131–146.

Nowicki, T., 1996. *Geologia jaskini Szczelina Chochołowska, Wyżnia Brama Chochołowska, Tatry Zachodnie.* Przyroda TPN a Człowiek, t. I, Kraków-Zakopane, pp. 102–104.

Plagnes, V., Causse, C., Genty, D., Paterne, M., Blamart, D., 2002. A discontinuous climatic record from 187 to 74 ka from a speleothem of the Clamouse Cave (south of France). *Earth and Planetary Science Letters* 201, 87–103.

Railsback, L.B., Gibbard, P.L., Head, M.J., Voarintsoa, N.R.G., Toucanne, S., 2015. An optimized scheme of lettered marine isotope substages for the last 1.0 million years, and the climatostratigraphic nature of isotope stages and substages. *Quaternary Science Reviews* 111, 94–106.

Regattieri, E., Zanchetta, G., Isola, I., Bajo, P., Perchiazzi, N., Drysdale, R.N, Boschi, C., Hellstrom, J.C, Francke, A., Wagner, B., 2018. A MIS 9/MIS 8 speleothem record of hydrological variability from Macedonia (F.Y.R.O.M.). *Global and Planetary Change* 162, 39–52.

Roe, H.M., Coope, G.R., Devoy, R.J.N., Harrison, C.J.O., Penkman, K.E.H., Preece, R.C., Schreve, D.C., 2009. Differentiation of MIS 9 and MIS 11 in the continental record: vegetational, faunal, aminostratigraphic and sea-level evidence from coastal sites in Essex, UK. *Quaternary Science Reviews* 28, 2342–2373.

Różański, K., Araguás-Araguás, L., Gonfiantini, R., 1993. Isotopic patterns in modern global precipitation. In: Swart, P.K.,

Lohmann, K.C., McKenzie, J., Savin, S., (Eds.), *Climate Change in Continental Isotopic Records*, Geophysical Monograph 78, American Geophysical Union, Washington, DC, pp. 1–36.

Różański, K., Duliński, M., 1988. A reconnaissance study of water in the karst of the Western Tatras Mountains. *Catena* 15, 289–301.

Ruddiman, W.F., 2007. The early anthropogenic hypothesis: challenges and responses. *Reviews of Geophysics* 45. http://dx.doi.org/10.1029/2006RG000207.

Sadori, L., Koutsodendris, A., Panagiotopoulos, K., Masi, A., Bertini, A., Combourieu-Nebout, N., Francke, A., *et al.*, 2016. Pollen-based paleoenvironmental and paleoclimatic change at Lake Ohrid (south-eastern Europe) during the past 500 ka. *Biogeosciences* 13, 1423–1437.

Sharp, Z., 2017. *Principles of Stable Isotope Geochemistry*, 2nd ed. Pearson Prentice Hall, Upper Saddle River, NJ.

Spötl, C., Mangini, A., 2007. Speleothems and paleoglaciers. *Earth and Planetary Science Letters* 254, 323–331.

Spötl, C., Mangini, A., Richards, D.A., 2006. Chronology and paleoenvironment of marine isotope stage 3 from two high-elevation speleothems, Austrian Alps. *Quaternary Science Reviews* 25, 1127–1136.

Spötl, C., Scholz, D., Mangini, A., 2008. A terrestrial U/Th-dated stable isotope record of the penultimate Interglacial. *Earth and Planetary Science Letters* 276, 283–292.

Szczygieł, J., Mendecki, M., Hercman, H., Wróblewski, W., Glazer, M., 2019. Relict landslide development as inferred from speleothem deformation, tectonic data, and geoelectrics. *Geomorphology* 330, 116–128.

Tesoriero, A.J., Pankow, J.F., 1996. Solid solution partitioning of Sr^{2+}, Ba^{2+} and Cd^{2+} into calcite. *Geochimica et Cosmochimica Acta* 60, 1053–1063.

Tooth, A.F., Fairchild, I.J., 2003. Soil and karst aquifer hydrological controls on the geochemical evolution of speleothem-forming drip waters, Crag Cave, southwest Ireland. *Journal of Hydrology* 273, 51–68.

Treble, P.C., Chappell, J., Shelley, J.M.G., 2005. Complex speleothem growth processes revealed by trace element mapping and scanning electron microscopy of annual layers. *Geochimica et Cosmochimica Acta* 69, 4855–4863.

Treble, P.C., Shelley, J.M.G., Chappell, J., 2003. Comparison of high resolution sub-annual records of trace elements in a modern (1911–1992) speleothem with instrumental climate data from southwest Australia. *Earth and Planetary Science Letters* 216, 141–153.

Tremaine, D.M., Froelich, P.N., Wang, Y., 2011. Speleothem calcite farmed in situ: modern calibration of $\delta^{18}O$ and $\delta^{13}C$ paleoclimate proxies in a continuously-monitored natural cave system. *Geochimica et Cosmochimica Acta* 75, 4929–4950.

Urban, B., 2007. Interglacial pollen records from Schöningen, North Germany. In: Sirocko, F., Litt, T., Claussen, M., Sanchez-Goni, M.F. (Eds.), *The Climate of Past Interglacials.* Development in Quaternary Science 7, Elsevier, Amsterdam, pp. 417–444.

van Beynen, P.E., Soto, L., Pace-Graczyk, K., 2008. Paleoclimate reconstruction derived from speleothem strontium and $\delta^{13}C$ in central Florida. *Quaternary International* 187, 76–83.

Yin, Q., Berger, A., 2015. Interglacial analogues of the Holocene and its natural near future. *Quaternary Science Reviews* 120, 28–46.

Zhang, Z., 2018. *Multivariate Time Series Analysis in Climate and Environmental Research.* Springer International Publishing, Cham, Switzerland.